Nanoscale structural evolution of Al2Cu precipitates in friction-stir welded Al–Cu–Mg alloy

Nanoscale structural evolution of Al2Cu precipitates in friction-stir welded Al–Cu–Mg alloy

I Zuiko*, S Malopheyev, S Mironov, R Kaibyshev

Laboratory of Mechanical Properties of Nanostructured Materials and Superalloys, Belgorod National Research University. Belgorod 308015, Pobeda str. 85, Russia

*Corresponding author: zuiko.ivan@gmail.com

Abstract. The work is devoted to FSW of cold rolled AA2519. The non-uniform distribution of all second phase precipitates (including coherent θ″ and non-coherent θ) was shown *via* the TEM-technique. The nucleation of the stable θ-phase, along with decreased dislocation density, led to a drop (~60 $HV_{0.2}$) in the microhardness of the nugget zone.

1. Introduction

Over the past hundred years, age hardening in alloys has been successfully exploited on an industrial scale to strengthen materials. For example, the most remarkable improvements in strength of Al–Cu–Mg alloys (i.e., 2XXX-series) are obtained through the formation of secondary precipitates in course of ageing. Previous studies [1-8] showed that precipitation scenario in Al–Cu–Mg alloys (with Cu/Mg ratio >5.6) could be represented as follows:

$$SSSS \rightarrow \{001\} \text{ clusters} \rightarrow \text{GP zones } (Al_3Cu) \rightarrow \theta'' (Al_2Cu) \rightarrow \theta' (Al_2Cu) \rightarrow \theta (Al_2Cu) \quad (1)$$

$$\{111\} \text{ clusters} \rightarrow \Omega (Al_2Cu) \rightarrow \theta' (Al_2Cu) \quad (2)$$

where SSSS stands for supersaturated solid solution and GP stands for Guinier-Preston zones. The first and second sequences occur on $\{100\}_\alpha$ and $\{111\}_\alpha$, respectively [2-5].

Now it is realized that to obtain maximum benefits in terms of strength, the age-hardened Al–Cu–Mg alloys need to be subjected to thermo-mechanical treatment which includes solid solution treatment, cold working and subsequent artificial ageing. Usually, a straighten procedure is applied to relieve the residual stress induced by quenching. But materials used in industry should demonstrate weldability. Experience has shown that this could be produced by applying a solid-state joining process called friction stir welding (FSW). However, in age hardening alloys, the heat generated during FSW causes the evolving of grains, secondary phases and crystalline defects (which affect the mechanical properties). Essentially, the weld microstructure is determined by the thermal cycle, which can be varied by changing the welding parameters (primarily, the tool travel speed and spindle rate). It should be mentioned that FSW generates a non-homogeneous distribution of temperature and, hence, a mixed (non-homogeneous) microstructure appears. Typically, it consists of a base material, a heat affected zone, a thermo-mechanically affected zone and a stir zone.

The deformation process associated with the welding procedure is very complicated and involves recovery and continuous dynamic recrystallization. The precipitation phenomenon in heat-treatable aluminium alloys is sophisticated and includes dissolution, coarsening and phase transformations. All aforementioned processes are complicated by the presence of a large quantity of crystalline defects (first

of all deformation induced vacancies, dislocations and moving boundaries), which are unequivocally affected.

In the most cases, FSW is applied to completely treated (aged) material. It is thought that in the thermo-mechanically affected zone and the stir zone, the precipitates are dissolved, whereas in the heat-affected zone, particle coarsening occurs. Therefore, the demand for improving their properties is an urgent scientific challenge. The authors hypothesized that the production of high-quality welds of heat-treatable Al alloys may be possible through applying FSW after solution treatment and cold deformation. In this case, the thermal cycle will be similar to ageing. To further increase the strength characteristics, the use of post-weld ageing is proposed. As far as the authors know, this processing strategy has never been used before.

2. Methodology

The nominal chemical composition of the used AA2519 is Al–5.64Cu–0.33Mn–0.23Mg–0.15Zr-0.11Ti–0.09V–0.08Fe–0.08Zn–0.04Sn–0.01Si (in weight %). An ingot of the alloy with dimensions of 30×100×120 mm^3 was homogenized (24 hours at 510°C) and hot rolled (T=425°C) to a thickness of 12 mm ($\varepsilon \sim 0.88$). Next, plates with a thickness of 3.75 mm, a width of 50 mm, and a length of 150 mm were cut, treated with a solid-solution at 535°C for 1h, quenched in water and rolled at room temperature to a total thickness reduction of 20% ($\varepsilon \sim 0.22$). Then the rolled material was friction-stir butt welded using an AccuStir 1004 FSW machine operating in two opposite regimes:

a) "cold" (spindle rate of 500 rpm and tool travel speed of 380 mm/min);
b) "hot" (spindle rate of 1100 rpm and tool travel speed of 760 mm/min)

This division is based on the statement that the FSW is a function of process variables (primary traverse and rotation speeds) [4]. The welding tool was fabricated from tool steel and consisted of a shoulder of 12.5 mm in diameter and an M5 cylindrical probe (pin) of 1.9 mm in length. A tilting angle of 2.5° was employed in all cases. The rolling and welding directions were parallel to each other. Finally, for imparting peak ageing the welded plates were annealed at 165°C for 6 hours. The choice of the regime is based on the analysis of ageing curves, which were shown in the preliminary work [6]. To view the microstructure distribution in the welds (i.e. to define various microstructural zones), the midthickness microhardness profiles were measured. TEM experiments were carried out in the longitudinal plane containing the welding/rolling and normal directions. Foils were cut directly from the centre of the welds (i.e. from the nugget region) and prepared in a standard manner. Importantly, all microstructural observations were conducted on the post-weld heat-treated samples. In the SAED patterns, reflections from the θ′, θ″ and Ω phases are marked in green, blue and red colours, respectively. The schemes of indexed SAED patterns as well as other experimental details, could be found in Refs. [2-3, 5-6, 8].

3. Results and discussion

Figure 1 shows the microhardness profile measured across the welded joints in both the "cold-" and "hot-welded" conditions. Previously, we showed that after cold rolling with a reduction of 20% ($\varepsilon \sim 0.22$), the hardness of the alloy increased from 96±1 $HV_{0.2}$ (after solid solution treatment) to 155±1 $HV_{0.2}$. Subsequent age hardening (165°C for 6 hours) leads to a further increase in hardness to 167±1 $HV_{0.2}$. After both types of the welding process, the hardness-distance curves can roughly be divided into three sections. In the first (15-7mm) the hardness of the alloy remains approximately constant. Then the curves (7-3 mm) show a monotonic decrease to ~120 $HV_{0.2}$ and a rapid drop to minimal values (3-0 mm). Usually, such trends in microhardness are typical for non-heat treatable alloys (see Figure 23 in Ref [4]). Obviously, changes in the transverse hardness are associated with various microstructure features (dislocation densities, grains sizes, phase composition).

The TEM technique was employed to interpret the observed drop in microhardness in nugget. The aim of these investigations was to characterize the grain structure, dislocation and precipitation state. The SAED patterns after cold deformation [2,5] contain only diffraction spots from the Al matrix, and no evidence of any precipitates in the images could be discerned. In the meantime, after peak-ageing

(Figure 2), TEM-images and SAED patterns provide robust evidence for the presence of two variants of θ″/θ′ on orthogonal sets of the {001} planes. In addition, the SAED patterns exhibit intensity maxima at 1/3 and 2/3 $[220]_\alpha$ (red circles in the inset in Figure 2a) that is a feature (peculiarity) of the Ω-phase. A TEM-micrograph taken along the $<011>_\alpha$ directions, as well as streaking along $\{111\}_\alpha$, unequivocally confirm the presence of two variants of fine plate-shaped Ω-precipitates lying on the $\{111\}_\alpha$ planes of the matrix.

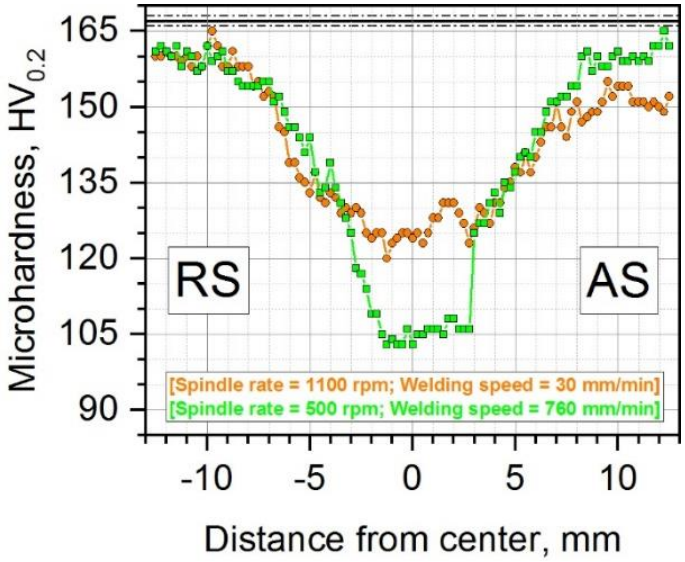

Figure 1. Microhardness profiles measured across transverse cross-sections of the welds. RS and AS denote retreating side and advancing sides, respectively.

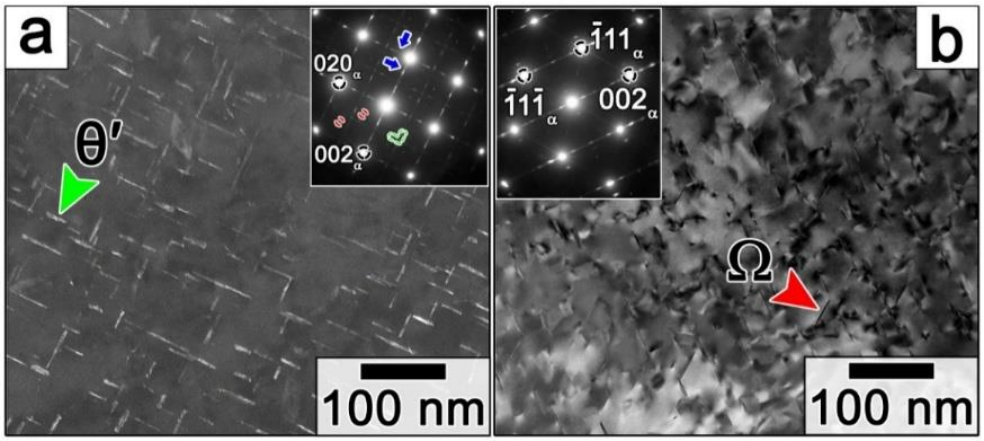

Figure 2. Intragranular precipitation of secondary precipitates in the peak aged alloy. In (a) and (c) the electron beam was parallel to the $<001>_\alpha$ and $<011>_\alpha$ directions, respectively.

To compare the microstructural evolution as the function of the welding conditions, we introduce Figures 3 and 4, which represent a series of TEM-micrographs together with the corresponding SAED patterns obtained from the stir zone. Th diversity of the second phases in these conditions is fascinating. Apart from the non-homogeneous distribution of the coherent θ″-phase (Figures 3b, 4b), the analysis of SAED patterns, as well as EDX measurements (not shown) point out to the precipitation of the incoherent θ-phase. It should be noted that traditionally θ are nucleated in the interphase of θ′/matrix interfaces, grain boundaries (more than 9°) or directly from the matrix if the ageing temperature is high enough (i.e. >300°C) [7]. Consequently, it could be assumed that copper available for precipitation has to be shared between the strengthening θ″/θ′/Ω particles and the stable θ-phase. Also, it should be

mentioned that presence of θ has a deleterious effect on the mechanical properties (tended to the enhanced corrosion along the rows of particles, reduction of the fatigue resistance of the material).

4. Conclusions

We have investigated the mechanical properties and the related microstructure of the friction stir welded and aged Al–Cu–Mg alloy. The major results are as follows:

1. Ageing after FSW of cold rolled AA2519 is an ineffective way to gain qualitative welds. This is due to the nugget does not contain sufficient solute capable of sustaining subsequent metastable precipitation and age hardening.
2. FSW makes θ formation easier by providing a great number of possible sites for heterogeneous nucleation.
3. The low hardness of the nugget zone is attributed to the low dislocation density and the non-homogeneous distribution of all precipitates (including coherent θ″ and stable θ), as revealed by transmission electron microscopy.

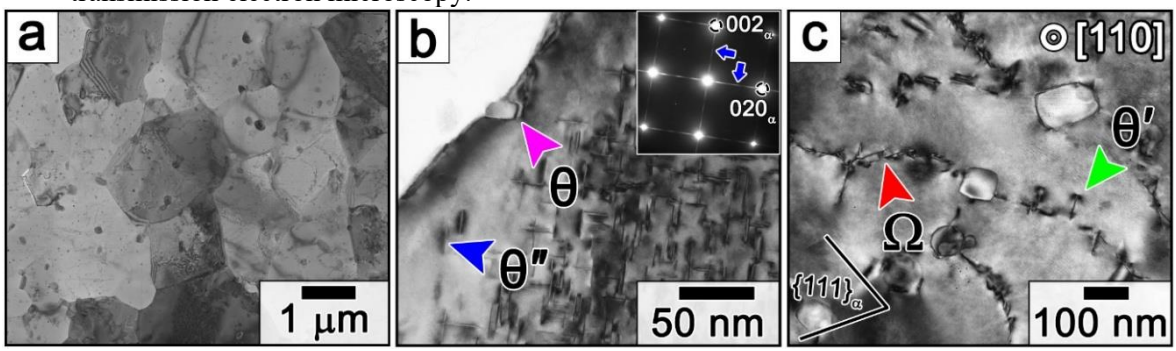

Figure 3. BF-TEM micrographs and corresponding SAED patterns of the “cold” weld.

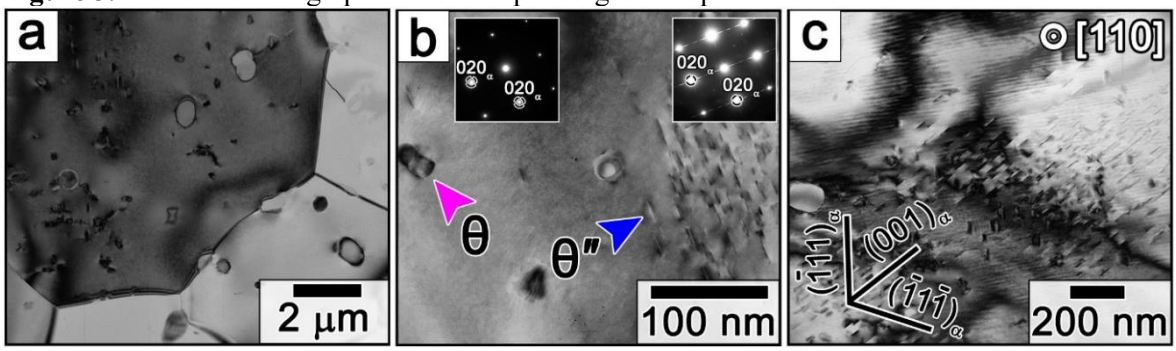

Figure 4. BF-TEM micrographs and corresponding SAED patterns of the “hot” weld.

References

[1] Palmer I, John D St, Nie J F, Qian M, Light Alloys: Metallurgy of the Light Metals, 5th ed., Butterworth-Heinemann, 2017
[2] Zuiko I, Gazizov M, Kaibyshev R, 2018 *Def. and Diff.* For. **385** 290
[3] Zuiko I, Gazizov M, Kaibyshev R, 2014 *Mater. Sci. For.*, **794–796** 888
[4] Threadgill P L, Leonard A J, Shercliff H R, Withers P J, 2009 *Int. Mat. Rev.* **54** 49
[5] Zuiko I, Kaibyshev R, 2018 *Mater. Sci. Eng.* A **737** 401
[6] Zuiko I S, Mironov S, Kaibyshev R, 2020 *Mater. Sci. Eng. A* **793** 139882
[7] Wang S C, Starink M J, 2005 *Int. Mat. Rev.* **50** 193
[8] Zuiko I, Kulitskii V, Kaibyshev R, 2018 *Def. and Diff. For.* **385** 364